Visualizing Chemical Reactions and Crossover Processes in a Fuel Cell Inserted in the ESR Resonator: Detection by Spin Trapping of Oxygen Radicals, Nafion-Derived Fragments, and Hydrogen and Deuterium Atoms

Marek Danilczuk,[†] Frank D. Coms,[‡] and Shulamith Schlick[†,*]

Department of Chemistry and Biochemistry, University of Detroit Mercy, 4001 West McNichols Road, Detroit, Michigan 48221, and General Motors Fuel Cell Research Laboratories, 10 Carriage Street, Honeoye Falls, New York 14472

Received: February 20, 2009; Revised Manuscript Received: April 22, 2009

We present experiments in an in situ fuel cell (FC) inserted in the resonator of the ESR spectrometer that offered the ability to observe separately processes at anode and cathode sides and to monitor the formation of $HO^{\bullet}$ and $HOO^{\bullet}$ radicals, $H^{\bullet}$ and $D^{\bullet}$ atoms, and radical fragments derived from the Nafion membrane. The presence of the radicals was determined by spin-trapping electron spin resonance (ESR) with 5,5-dimethylpyrroline *N*-oxide (DMPO) as a spin trap. The in situ FC was operated at 300 K with a membrane−electrode assembly (MEA) based on Nafion 117 and Pt as catalyst, at closed and open circuit voltage conditions, CCV and OCV, respectively. Experiments with H_2 or D_2 at the anode and O_2 at the cathode were performed. The DMPO/OH adduct was detected only at the cathode for CCV operation, suggesting generation of hydroxyl radicals from H_2O_2 formed electrochemically via the two-electron reduction of oxygen. The DMPO/OOH adduct, detected in this study for the first time in a FC, appeared at the cathode and anode for OCV operation, and at the cathode after CCV FC operation of ≥2 h. These results were interpreted in terms of electrochemical generation of $HOO^{\bullet}$ at the cathode ($HO^{\bullet} + H_2O_2 \rightarrow H_2O + HOO^{\bullet}$) and its chemical generation at the anode from hydrogen atoms and crossover oxygen ($H^{\bullet} + O_2 \rightarrow HOO^{\bullet}$). DMPO/H and DMPO/D adducts were detected at the anode and cathode sides, for CCV and OCV operation; $H^{\bullet}$ and $D^{\bullet}$ are aggressive radicals capable of abstracting fluorine from the tertiary carbon in the polymer membrane chain and of leading to chain fragmentation. Carbon-centered radical (CCR) adducts were detected at the cathode after CCV FC operation; weak CCR signals were also detected at the anode. CCRs can originate only from the Nafion membranes, and their presence indicates membrane fragmentation. Taken together, this study has demonstrated that FC operation involves processes such as gas crossover, reactions at the catalyst surface, and possible attack of the membrane by reactive $H^{\bullet}$ or $D^{\bullet}$ that do not occur in ex situ experiments in the laboratory, thus implying different mechanistic pathways in the two types of experiments.

Introduction

Fuel cells, which transform the chemical energy from the reaction between H_2 and O_2 into electrical energy, have the potential to become alternative sources of clean energy for automotive and stationary applications.[1,2] Key components of a fuel cell (FC) are the electrodes, the catalyst, and the proton exchange membrane (PEM), which is a polymer modified to include ions, typically sulfonic groups: an *ionomer*.[3] In the presence of water, ionomers self-assemble into microphase-separated domains that allow the movement of H^+ from the anode to the cathode. The membrane role and performance were demonstrated by Nafion (Chart 1), the ionomer that consists of a perfluorinated backbone (for chemical stability) and pendant chains terminated by sulfonic groups, SO_3H (for ionic conductivity).[3,4] The conductive properties of Nafion and of other FC membranes depend on the water content and the equivalent weight (EW); the latter is the dry ionomer mass that contains 1 mol of sulfonic groups.[5,6]

Although FCs typically operate at ≈350 K, important advantages can be gained by operating at higher temperatures, ≈390 K; this temperature imposes additional stringent requirements in terms of membrane stability. Even at an operating temperature of ≈320 K, evidence for the deterioration of Nafion membranes was detected by X-ray powder diffraction (XRD) and X-ray photoelectron spectroscopy (XPS).[7] Membrane durability has become a major issue and obstacle in the wide adoption of fuel cell-powered vehicles. Work in various laboratories has demonstrated the formation of a small amount of hydrogen peroxide during the two-electron oxygen reduction at the cathode side of the fuel cell, reaction 1. H_2O_2 can dissociate into two hydroxyl radicals ($HO^{\bullet}$, reaction 2) and react with $HO^{\bullet}$ to form hydroperoxyl radicals ($HOO^{\bullet}$, reaction 3).

CHART 1: Nafion 117, EW 1100, $m = 6.5$

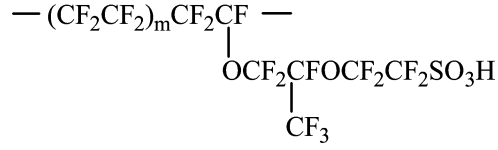

$$O_2 + 2H^+ + 2e^- \rightarrow H_2O_2$$
(electrochemical route of H_2O_2 formation) (1)

* Corresponding author. Tel.: 1-313-993-1012. Fax: 1-313-993-1144. E-mail: schlicks@udmercy.edu.
[†] University of Detroit Mercy.
[‡] General Motors Fuel Cell Research Lab.

10.1021/jp901597f CCC: $40.75
Published on Web 05/19/2009

$$H_2O_2 \rightarrow HO^{\bullet} \quad \text{(on traces of transition metal cations or at catalyst)} \qquad (2)$$

$$H_2O_2 + HO^{\bullet} \rightarrow HOO^{\bullet} + H_2O \qquad (3)$$

When hydroxyl radicals are generated in the laboratory by UV irradiation of hydrogen peroxide, reaction 4 below is also expected:

$$HOO^{\bullet} + H_2O \rightleftarrows O_2^{\bullet -} + H_3O^{+} \qquad (4)$$

However, at the low pH of a fuel cell, ≈1, the concentration of the superoxide radical, $O_2^{\bullet -}$, is very low: for $pK_a = 4.7$ for the above reaction, the concentration ratio $[HOO^{\bullet}]/[O_2^{\bullet -}]$ is ≈5000, and the relative concentrations are 99.98% for $HOO^{\bullet}$ and 0.02% for $O_2^{\bullet -}$, respectively. *Therefore ionization of HOO•, reaction 4, is not significant for a FC.*

The formation of HO• via the Haber−Weiss process, reaction 5, may also be considered.

$$O_2^{\bullet -} + H_2O_2 \rightarrow HO^{\bullet} + HO^{-} + O_2 \qquad (5)$$

The reaction is very slow but important as a source of oxidative stress in biological systems, and is catalyzed by the reduction of Fe(III) to Fe(II) followed by the Fenton reaction. This source for HO• radicals is not expected in a fuel cell, both because of the low concentration of superoxide radicals as well as due to the negligible concentrations of Fe(II) and Fe(III). For the low pH of a fuel cell, it is more appropriate to express the Haber−Weiss process in terms of the HOO• radical, reaction 5a:

$$HOO^{\bullet} + H_2O_2 \rightarrow HO^{\bullet} + H_2O + O_2 \qquad (5a)$$

In Table 1 we have collected the reaction rate constants and corresponding references for the most important reactions mentioned in this paper, and the equilibrium constant (pK_a) for reaction 4. The Haber−Weiss process is expressed there in terms of HOO•, reaction 5a.

It is commonly accepted that degradation processes of perfluorosulfonic acid (PFSA) membranes such as Nafion are mediated by oxygen radicals.[8−11] Numerous studies have documented that chemical degradation reactions involve abstraction of hydrogen atoms bound to either oxygen or carbon during both initiation and propagation steps. A detailed thermochemical and kinetic analysis revealed that only HO• is capable of removing these hydrogen atoms;[11] however, HOO• radicals can also be involved in degradation reactions but not as an initiator. The higher reactivity of HO• relative to HOO• is reflected in their respective reduction potentials (2.59 vs 1.48 V) and the O−H bond strengths of their corresponding reduced forms H_2O and H_2O_2 (497 vs 369 kJ/mol).[11]

The degradation mechanism in Nafion and other membranes used in FCs has been investigated in ex situ experiments by generating reactive oxygen intermediates in the laboratory via the Fenton reaction,[12] the photo-Fenton reaction,[13] and UV irradiation of H_2O_2.[14] The results for the membranes have been also evaluated by comparison with the behavior of model compounds.

The rate of membrane degradation during fuel cell operation, "in situ" experiments, is usually determined by measuring the fluoride ion content in the exhaust water, but ^{19}F NMR spectroscopy, size exclusion chromatography (SEC), mass spectrometry (MS), and liquid chromatography−MS (LC-MS) have also been applied. The degradation mechanism that has gained much support is chemical attack by hydroxyl radicals on carboxylic end groups present as impurities in perfluorinated membranes.[11,15−20] This reaction leads to the unzipping of the polymer chain, with concomitant loss of one carbon in each step of the reaction between the COOH group and HO•. While this mechanism has been supported by some experimental results, current results (including our studies) have suggested that main chain end group attack is not the only mechanism: degradation by side-chain attack is an additional possibility given the large number of pendant chains, especially when the level of chain-end COOH impurities is low.[20] A general conclusion from several studies was that lifetimes of PEMs deduced from laboratory tests are longer compared to those of the same membranes in actual FC conditions. It appears that present procedures are suitable only for a relative ranking of membranes in terms of their stability.

We have developed direct electron spin resonance (ESR) and spin-trapping methods for the detection and identification of oxygen radicals as well as specific radical intermediates formed in Nafion and model compounds upon exposure to oxygen radicals in the laboratory.[21−27] The major objectives of these studies were to determine the presence and identify the structure of radicals produced as a result of specific membrane treatments; to develop laboratory protocols for the study of membrane degradation that correlate well with the extent of degradation produced during automotive operating conditions; and to formulate the degradation mechanism. ESR methods are particularly suitable for this investigation, because of their sensitivity and specificity for the detection of radical species. Direct ESR detection was carried out at low temperatures, or by progressive annealing to higher temperatures, in order to establish the lifetimes and reactivity of various intermediate radicals and to follow their disappearance or transformation to other species.[21,22,25,26] For short-lived radicals at room temperature, spin-trapping ESR methods were used;[28−30] these methods are based on scavenging of short-lived radicals, R•, by spin traps, and formation of more stable radical adducts, usually nitroxide radicals, as illustrated in Scheme 1 for 5,5-dimethylpyrroline *N*-oxide (DMPO), a nitrone spin trap. In most cases, the ESR spectra of spin adducts of nitrone spin traps exhibit hyperfine splittings (hfs) from ^{14}N and Hβ nuclei. By analyzing the magnetic parameters of adducts, it is often possible to identify the type of radicals that were trapped. Nitroso and nitrone as spin traps have been used extensively for the detection of unstable intermediates in biological systems. Our spin trapping studies represent the adaptation and extension of spin trapping techniques to polymeric systems.[23,25,27]

SCHEME 1: Spin Trapping by 5,5-Dimethyl-1-pyrroline *N*-oxide (DMPO)

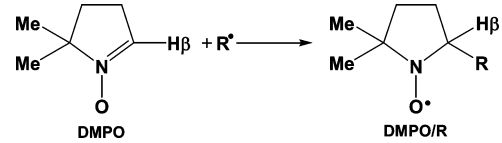

In Nafion membranes partially neutralized by Fe(II) and UV-irradiated in the presence of H_2O_2 (the photo-Fenton reaction[13]),

TABLE 1: Reaction Rate Constants

reaction	$k/M^{-1}\ s^{-1}$	reference
3 $H_2O_2 + HO^\bullet \rightarrow H_2O + O_2^{\bullet-}$ (HOO$^\bullet$)	2.7×10^7 solvent: H_2O, pH = 7.8, 293 K	Buxton, G. V.; Greenstock, C. L.; Helman, W. P.; Ross, A. B. *J. Phys. Chem. Ref. Data* **1988,** *17,* 513−886
		Christensen, H.; Sehested, K.; Corfitzen, H. *J. Phys. Chem.* **1982,** *86*, 1588−1590
	2.0×10^7 reference reaction: $HO^\bullet + SCN^- \rightarrow$ solvent: H_2O, pH = 7	Greenstock, C. L.; Wiebe, R. H. *Oxygen and Oxy-Radicals in Chemistry and Biology*; M. A. J. Rodgers and E. L. Powers, Eds.; Academic Press: New York, 1981; pp 119−31
	3.8×10^7 reference reaction: $HO^\bullet$ + luminol → solvent: H_2O, pH = 7.7− 11	Merenyi, G.; Lind, J. S. *J. Am. Chem. Soc.* **1980,** *102*, 5830−5835
	2.4×10^7 reference reaction: $HO^\bullet + I^- \rightarrow$ solvent: H_2O, pH = 7	Thomas, J. K. *Trans. Faraday Soc.* **1965,** *61,* 702−707
	2.7×10^7 solvent: H_2O, pH = 7.8, 293 K	Buxton, G. V.; Greenstock, C. L.; Helman, W. P.; Ross, A. B. *J. Phys. Chem. Ref. Data* **1988,** *17,* 513−886
4 $HOO^\bullet + H_2O \leftrightarrow O_2^{\bullet-} + H_3O^+$	pK_a = 4.7[a]	Bielski, B. H. J. *Photochem. Photobiol.* **1978**, *28,* 645−649
5a $HOO^\bullet + H_2O_2 \rightarrow HO^\bullet + H_2O + O_2$	0.5−3.0	(a) Weinstein, J.; Bielski, B. H. J. *J. Am. Chem. Soc.* **1979,** *101*, 58−62. (b) Koppenol, W. H.; Butler, J.; van Leeuwen, J. W. *Photochem. Photobiol.* **1978**, *28,* 655−660
7 $HO^\bullet + H_2 \rightarrow H_2O + H^\bullet$	3.4×10^7 reference reaction: $HO^\bullet + Cu^{2+} \rightarrow$ solvent: H_2O, pH =5.3, 293 K	Christensen, H.; Sehested, K. *J. Phys. Chem.* **1983,** *87*, 118−120
	4.0×10^7 solvent: H_2O, pH = 4.7, 298 K	Schmidt, K. H. *J. Phys. Chem.* **1977**, *81*, 1257−1263
	3.5×10^7 solvent: H_2O	Thomas, J. K. *Trans. Faraday Soc.* **1965,** *61,* 702−707
	6.0×10^7 pH ≈ 1, T = 298 K reference reaction: $HO^\bullet + Fe^{2+} \rightarrow$	Bunn, D.; Dainton, F. S.; Salmon, G. A.; Hardwick, T. J. *Trans. Faraday Soc.* **1959**, *55*, 1760−1767.
	4.2×10^7	Buxton, G. V.; Greenstock, C. L.; Helman, W. P.; Ross, A. B. *J. Phys. Chem. Ref. Data* **1988,** *17,* 513−886. IUPAC Subcommittee on Gas Kinetic Evaluation for Atmospheric Chemistry, App, Enthalpy Data; http://www.iupac-kinetic.ch.cam.ac.uk/thermo2003.pdf
8 $H^\bullet + O_2 \rightarrow HOO^\bullet$	1.2×10^{10} solvent: H_2O	Buxton, G. V.; Greenstock, C. L.; Helman, W. P.; Ross, A. B. *J. Phys. Chem. Data. ref* **1988,** *17,* 513−886.
	1.0×10^{10} reference reaction: $H^\bullet + MnO_4^- \rightarrow$ solvent: H_2O, pH = 2, 298 K	Elliot, A. J.; McCracken, D. R.; Buxton, G. V.; Wood, N. D. *J. Chem. Soc. Faraday Trans.* **1990,** *86*, 1539−1547.
	1.4×10^{10} reference reaction: $H^\bullet + Fe(CN)_6^{3-} \rightarrow$ solvent: H_2O, pH ≈ 1.9, 298 K	Elliot, A. J. *Radiat. Phys. Chem.* **1989,** *34*, 753−758.
	2.1×10^{10} solvent: H_2O	Gordon, S.; Hart, E. J.; Thomas, J. K. *J. Phys. Chem.* **1964,** *68*, 1262−1264.
9 $HOO^\bullet + HOO^\bullet \rightarrow H_2O_2 + O_2$	8.6×10^5	Bielski, B. H. J. *Photochem. Photobiol.* **1978**, *28,* 645−649.

[a] This value allows the calculation of HOO$^\bullet$ and $O_2^{\bullet-}$ concentrations at a given pH.

strong signals from a chain-end radical $RCF_2CF_2^\bullet$ were detected.[22] In subsequent experiments with Nafion membranes neutralized by Fe(III), the $RCF_2CF_2^\bullet$ radicals were detected even in the absence of H_2O_2, indicating that one of the roles of H_2O_2 is oxidation of Fe(II) to Fe(III). In ref 22 we have also proposed the well-documented direct reaction between Fe(III) and sulfonic groups: $-OCF_2CF_2SO_3^- + Fe(III) \rightarrow -OCF_2CF_2SO_3^\bullet + Fe(II)$, finally generating SO_3 and $-OCF_2CF_2^\bullet$. Fitting of the ESR spectrum together with density functional theory (DFT) calculations has indicated that the radical formed is $ROCF_2CF_2^\bullet$, as expected from a radical derived from the side chain of Nafion, not $RCF_2CF_2CF_2^\bullet$, if its origin is the main chain. Additional support for this assignment was obtained from exposure of a model compound that mimics the Nafion side chain, perfluoro(2-ethoxyethane)sulfonic acid ($CF_3CF_2OCF_2CF_2SO_3H$, PFEESA) to HO$^\bullet$ radicals generated by UV irradiation of H_2O_2.[27] In conclusion, our ex situ results have indicated that the Nafion side chain is vulnerable to attack by oxygen radicals. Strong support of this idea was reported recently in an in situ study of perfluorinated membranes by solid-state NMR spectroscopy; moreover, this study has suggested that "*the pendant side chains of the ionomers are more affected than the main chain*".[31]

At this stage in our work, it was imperative to compare the results of direct ESR and spin-trapping experiments with processes that occur in a FC. To this end, we initiated experiments in an in situ FC with a diameter of 5 mm that was inserted in the variable temperature insert of the resonator of the ESR spectrometer and allowed operation in the temperature range 100−400 K, under closed and open circuit voltage conditions, CCV and OCV, respectively. Here we present results obtained with an in situ FC operated at 300 K. The presence of radicals was determined by spin trapping with DMPO as the

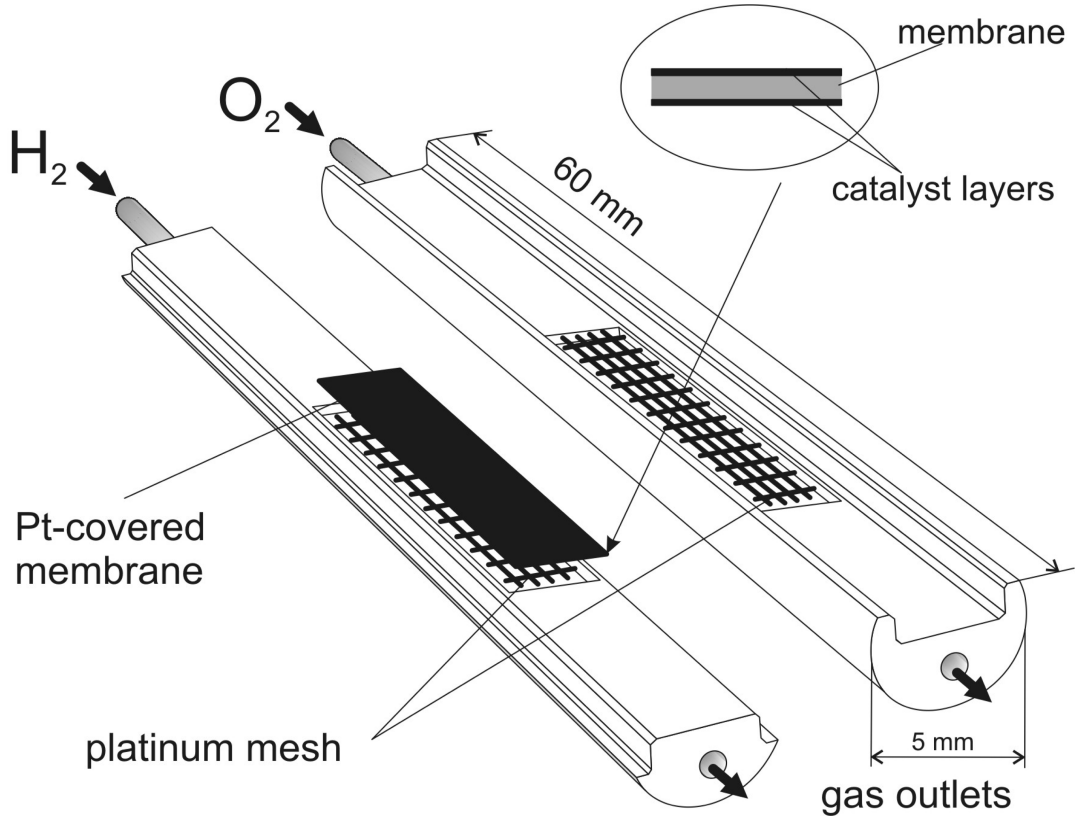

Figure 1. Schematic drawing of the in situ fuel cell.

spin trap. As described below, these experiments allowed the *separate* detection of radicals formed at the cathode and anode; identified at the cathode the presence of $HO^{\bullet}$ adducts and a Nafion-derived adduct for CCV conditions, and an $HOO^{\bullet}$ adduct for OCV conditions; and provided evidence for the presence of $H^{\bullet}$ and $D^{\bullet}$ adducts and for crossover of H_2 and D_2 from the anode to the cathode, and of O_2 from the cathode to the anode.

Experimental Section

Materials. DMPO was purchased from Sigma-Aldrich (97%), or synthesized in our laboratory and purified by double vacuum distillation following published details.[32] Identical results were obtained for the two sources of the spin trap. The gases (H_2 99.99%, D_2 99.8%, O_2 99.6%), Pt mesh with $d = 0.1$ mm, and Ag wire with $d = 0.127$ mm were also from Sigma-Aldrich.

Membrane−electrode assemblies (MEAs) based on Nafion 117 (thickness 0.178 mm) and Pt as catalyst (coverage 0.2 mg/cm^2) were a gift from Cortney Mittelsteadt of Giner Electrochemical Systems, LLC, where they were prepared using the decal-transfer process: the Nafion solution (5 wt % alcohol-based from Ion Power, Inc.) and Pt black powder (Johnson Matthey Co.) were mixed in a 1:5 ratio by weight and diluted in an alcohol solution to a ratio of approximately 1:5:100 Nafion: Pt:solution by weight, followed by sonication. This "ink" was then spray-cast onto a heated (100 °C) perfluoroalkoxy copolymer $-(CF_2CF_2)_n-(CF_2CF(OCF_3))_m-$ (PFA) film (McMaster Carr Co.). The decals were weighed and the Pt content was then calculated. Decals of desired shapes were removed from the larger decal and pressed onto a dry membrane at 150 °C for 10 min.

In Situ Fuel Cell. The fuel cell consists of two half-cylinders made of polystyrene cross-linked with 1,4-divinylbenzene (Rexolite), with indentation where the membrane, the Pt mesh, and the electrodes were placed, as shown in Figure 1. The cell material is rigid but not brittle, and easy to machine. The fuel cell was inserted in the variable-temperature insert of the ESR spectrometer; the results presented here were obtained at 300 K, but temperature variation is possible and is planned for future experiments. The electrodes were connected to an HP E2377A multimeter by silver wires. The gas flows to the fuel cell, 2 cm^3/min for oxygen, and 4 cm^3/min for hydrogen and deuterium were controlled with Matheson 610A flow meters. The Pt-covered Nafion membrane (MEA) dimensions were 3×17 mm^2. Tuning of the spectrometer was performed with the MEA positioned parallel to the poles of the magnet, as in an ESR flat cell; the MEA position was not critical when starting the FC operation, but became critical when the water content increased during extended FC operation. Full details on the design and dimensions of the in situ FC are available from the authors upon request.

Spin Trapping of Radical Intermediates. Because of the low concentration and limited stability of radicals formed during fuel cell operation, the spin-trapping ESR method was used. DMPO was chosen as a spin trap because of its well-documented trapping ability and selectivity for oxygen radicals and for carbon-centered radicals (CCRs).[23,27−29] About 1 μL of the aqueous solution of the spin trap, concentration 4 M, was deposited at the cathode or anode side; the solvent was H_2O for H_2 at the anode, and D_2O for D_2 at the anode. In some experiments the spin trap was added just before starting the FC operation. In other experiments, the FC was operated for 120−360 min, followed by addition of the DMPO solution and restarting of the gas flows; the results are expected to reflect the effect of MEA "break in" and membrane hydration on the type of radicals and adducts formed. Each timed FC operation followed by spin trap addition is a separate experiment, with a new MEA sample. Weak signals were observed when DMPO was added even before the gases were reconnected after the

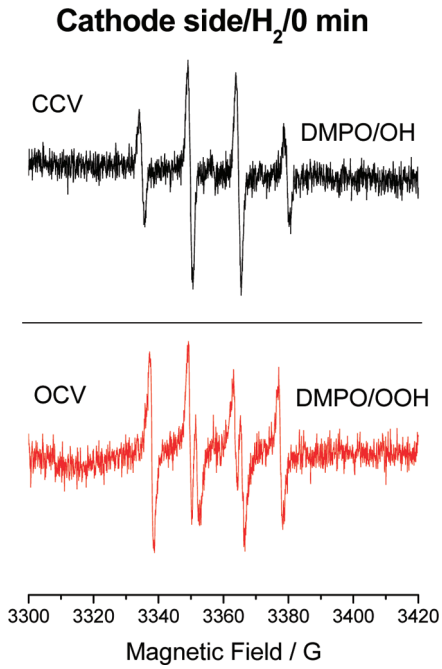

Figure 2. ESR spectra of DMPO adducts detected at the cathode side in the in situ FC when the spin trap was added just before CCV operation (top spectrum, "0 min") and OCV operation (lower spectrum). Modulation amplitude 2 G, receiver gain 4.48 × 10^5, 25 scans.

FC was operated for 120 min: for CCV conditions, the DMPO/OH adduct was detected at the cathode, and the DMPO/H at the anode; both signals were weak but identification was possible. For OCV conditions, the signals were much weaker even after 100 scans, but based on the total splitting we tentatively assigned the signals to the DMPO/OOH adduct at both cathode and anode.

ESR Measurements. ESR spectra were recorded at 300 K using Bruker X-band EMX spectrometers operating at 9.7 GHz and 100 kHz magnetic field modulation, and equipped with the Acquisit 32 Bit WINEPR data system version 3.01 for acquisition and manipulation, and the ER 4111 VT variable-temperature units. The microwave frequency was measured with the Hewlett-Packard 5350B microwave frequency counter. The hfs of the spin adducts were determined by fitting the spectra using the WinSim (NIEHS/NIH) simulation package;[33] the fitting also determines the relative intensity of each component for spectra that consist of a superposition of contributions from different adducts. Typical acquisition parameters for the ESR spectra were as follows: sweep width 150 G, microwave power 2 mW, time constant 20.48 ms, conversion time 41.94 ms, 2048 points, modulation amplitude 1 or 2 G, receiver gain in the range 4.48 × 10^5 to 1 × 10^6, and number of scans in the range 25−200. Specific ESR parameter sets are given for the spectra shown in Figures 2−5.

The Bruker ER 4105DR double rectangular X-band resonator was used for precise *g*-factor determination using a reference sample. The two coupled resonators ensure that both samples are measured under identical conditions, i.e., unchanged Q factors. All *g* values reported in Table 2 were measured with DPPH as a reference and rechecked with Cr(III) in a single crystal of MgO (g = 1.9797 at 300 K).

Results

The in situ experiments were performed with the fuel cell operated at closed circuit voltage (CCV) or open circuit voltage (OCV) conditions, with oxygen at the cathode and hydrogen or deuterium at the anode. No signals were detected before connecting the gases and addition of the spin trap solution on the membrane, or in the presence of the spin trap and the absence of the gases. The ESR spectra of DMPO adducts identified in the in situ fuel cell provided the evidence necessary to determine radical formation and trapping. The relative intensity of spin adducts and the corresponding magnetic parameters measured in the present study are summarized in Table 2. We emphasize that the relative intensities of the *adducts* given in Table 2 may not always reflect the corresponding intensities of the *radicals* that are formed, because of the different trapping rates of DMPO for the different radicals in the mixture.[34,35] Measurements of trapping rates for different radicals by DMPO and other spin traps will be the focus of additional studies in our laboratory.

Numerous experiments have convinced us that applying the spin trap solution at one electrode leads to the formation of adducts *at that electrode only*. Therefore, the results will be presented for DMPO applied on the cathode or anode side, with the corresponding gases fed at electrodes. Experimental ESR spectra are in black (CCV) and in red (OCV); simulated spectra are in blue.

Cathode Side (H_2/O_2). Figure 2 presents ESR spectra of adducts detected when the spin trap was added just before starting FC operation ("0 min"): DMPO/OH (CCV) and DMPO/OOH (OCV). Identification of these adducts is straightforward, based on the total range of the spectra (44.1 G for the $HO^•$ adduct and 39.4 G for the $HOO^•$ adduct) and on the splitting of the two middle lines in the $HOO^•$ adduct.[23] When the gas flows are stopped, signals from the DMPO/OH adduct can still be detected for about 30 min, and from the DMPO/OOH adduct for about 1 h. The lifetimes of these adducts may depend on the specific conditions in the system measured and their location in the inhomogeneous medium of a fuel cell, which consists of the gas diffusion layers, the electrodes, and the membrane.[26] The local conditions may affect both the rate of radical formation as well as the rate of spin trapping.

The DMPO/OH adduct was previously detected by Panchenko et al. at the cathode side of a Teflon in situ FC with Nafion as the membrane.[36,37] It is reasonable to assume that the formation of $HO^•$ radicals at the cathode is initiated electrochemically as a result of the two-electron oxygen reduction on the surface of the Pt catalyst that leads to H_2O_2 generation, reactions 1 and 2 above; the $HO^•$ radical can also be formed chemically by reactions 6, at the cathode catalyst from oxygen and crossover hydrogen, and at the anode catalyst from hydrogen and crossover oxygen:[38]

$$H_2 + O_2 \rightarrow 2HO^• \text{ (at the catalyst)} \qquad (6)$$

The DMPO/OOH adduct in a FC is detected in this study for the first time and can be formed from electrochemically generated H_2O_2 and reaction with hydroxyl radicals, reaction 3 above. Its detection at the cathode under OCV conditions may imply that the $HO^•$ radical is formed chemically (reaction 6) but reacts with crossover hydrogen to form $H^•$, which then reacts further with oxygen to generate the $HOO^•$ radical and the corresponding adduct, as in reactions 7 and 8 below.

$$HO^• + H_2 \rightarrow H_2O + H^• \qquad (7)$$

$$H^{\bullet} + O_2 \rightarrow HOO^{\bullet} \quad (8)$$

Another possibility for $HOO^{\bullet}$ formation involves the chemical generation of H_2O_2 at the anode from crossover O_2 followed by reaction of H_2O_2 with $HO^{\bullet}$ to give $HOO^{\bullet}$ and H_2O, reaction 3 above. For OCV conditions we must consider the chemical formation of H_2O_2 from O_2 and H_2 on the catalyst surface. In addition, we cannot exclude the possibility that some H_2O_2 is formed via $HOO^{\bullet}$ dismutation, reaction 9.

$$HOO^{\bullet} + HOO^{\bullet} \rightarrow H_2O_2 + O_2 \quad (9)$$

Reactions 6−8 imply crossover of hydrogen from the anode to the cathode in accord with the results presented below. Moreover, since $HO^{\bullet}$ is not detected at the anode, reaction 7 suggests that the concentration of H_2 is high enough to capture the $HO^{\bullet}$ radicals formed chemically via reaction 6. We will come back to the formation of $H^{\bullet}$ and of the DMPO/H adduct when discussing the results obtained with D_2 at the anode.

The evolution of ESR spectra of adducts when the spin trap was introduced to the cathode side just before CCV FC operation ("0 min") and after CCV operation times of 120, 240, and 360 min is shown in Figure 3A. The $HO^{\bullet}$ adduct is detected for "0" conditions. The dominant signal detected after 120 min of CCV operation is the DMPO/H adduct, with hfs from ^{14}N and from two equivalent ^{1}H nuclei.[39,40] However, weak signals from the DMPO/OH adduct can still be observed and are indicated by circles in Figure 3A; only three of the four lines of the DMPO/OH adduct are indicated, because the low-field line overlaps with a line from the DMPO/H adduct.

Experimental and simulated ESR spectra after 360 min of CCV operation are shown in Figure 3B. The experimental spectrum was simulated as a sum of three components that are also presented separately: the dominating signal is from the DMPO/OOH adduct (44%). The additional adducts were assigned to DMPO/H (36%) with a_N = 15.2 G, a_H= 20.2 G, (2H) and to DMPO/CCR (20%), the adduct of a carbon-centered radical, with a_N = 15.0 G and a_H= 21.4 G. This adduct is detected even after 240 min of FC operation, and its low-field signal is indicated by the downward arrow in Figure 3A. The hfs of all adducts are in line with literature data[23,27,39−46] and are presented in Table 2 together with their relative intensities. We note that the intensities deduced from the simulated sum vary somewhat from experiment to experiment, a result that is probably due to several factors: simulation of a complicated superposition of signals from several adducts; radical adducts with similar magnetic parameters, for example DMPO/OH and DMPO/OOH; and the general case of a weak spectrum that could not be automatically simulated by WinSim and had to be selected by visual inspection.

The detection of the $HOO^{\bullet}$ adduct at the cathode for OCV conditions therefore indicates the presence of the chemically formed $HOO^{\bullet}$ radical; for CCV operation the $HOO^{\bullet}$ presence suggests its formation from electrochemically formed H_2O_2 and its reaction with $HO^{\bullet}$.

TABLE 2: Hyperfine Splittings and *g* Values of DMPO Adducts Detected in the in Situ Fuel Cell, for Close Circuit Voltage (CCV, normal text) and Open Circuit Voltage (OCV, italic text) Conditions[a]

		hyperfine splittings, G				
system	adduct	a_N	a_H	a_D	*g* value	rel intensity, %
cathode/H_2/CCV/"0 min"	DMPO/OH	14.7	14.7		2.0057	
cathode/H_2/OCV/"0 min"	*DMPO/OOH*	*13.8*	*11.8*		*2.0036*	
(Figure 2)						
cathode/H_2/CCV/360 min	DMPO/H	15.2	20.2 (2H)		2.0057	36
(Figure 3)						
	DMPO/OOH	13.9	11.9		2.0036	44
	DMPO/CCR	15.0	21.4		2.0057	20
cathode/H_2/OCV/"0 min" or 360 min[b]	*DMPO/OOH*	*13.8*	*11.8*		*2.0036*	
cathode/D_2/CCV/"0 min"	DMPO/OOH or	14.0	12.4		2.0057	
(Figure 4A)						
	DMPO/OH	14.3	14.3		2.0057	
cathode/D_2/OCV/"0 min"[b]	*DMPO/OOH*	*14.0*	*12.0*		*2.0039*	
cathode/D_2/CCV/360 min	DMPO/OOH	14.1	13.6		2.0057	50
(Figure 4B)						
	DMPO/H	15.9	21.0 (2H)		2.0067	25
	DMPO/D	15.9	21.0	3.3	2.0055	15
	DMPO/CCR	15.6	22.0		2.0037	10
anode/H_2/CCV"0 min" or 120 min	DMPO/H	15.8	21.2 (2H)		2.0067	
(Figure 5A)						
anode/H_2/OCV"0 min" or 120 min	*DMPO/OOH*	*13.7*	*11.8*		*2.0067*	*72*
(Figure 5A)						
	DMPO/H	*15.6*	*21.0 (2H)*			*28*
anode/D_2/CCV/"0 min" or 120 min	DMPO/H	15.5	21.8 (2H)		2.0067	68
(Figure 5B)						
	DMPO/D	15.5	21.8	3.2	2.0067	32
anode/D_2/OCV/"0 min" or 120 min	*DMPO/OOH*	*13.9*	*11.8*		*2.0057*	*79*
(Figure 5B)						
	DMPO/H	*15.3*	20.1 (2H)		*2.0067*	*21*

[a] "0 min" indicates that the spin trap was added just before the start of the FC operation; and "120 min" and "360 min" mean that the spin trap was added after these times of FC operation. [b] Spectra not presented.

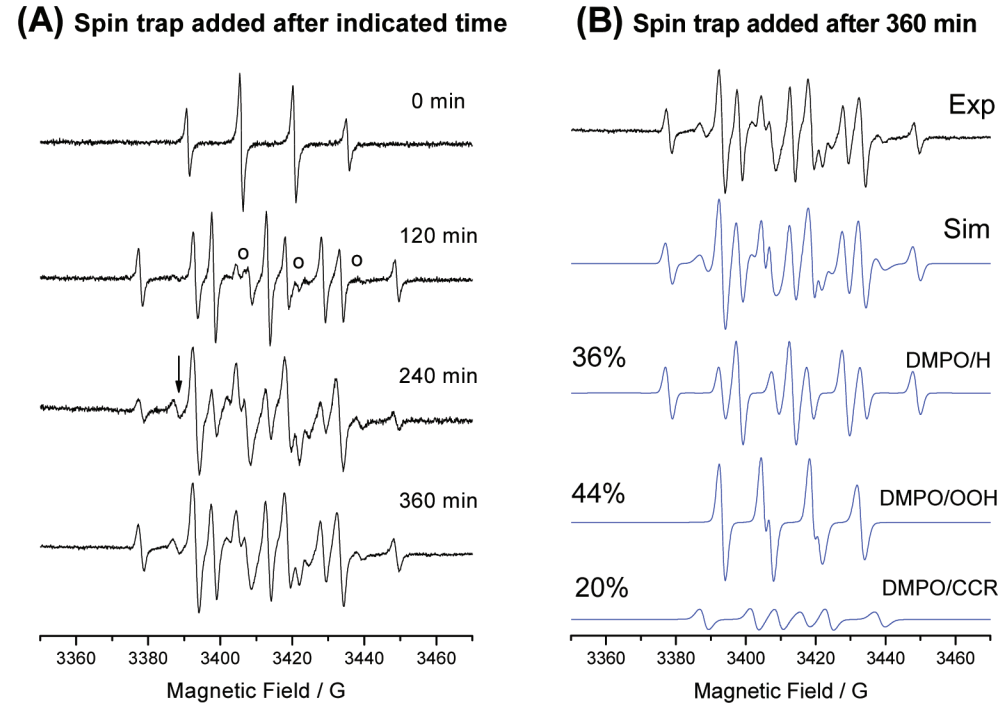

Figure 3. (A) Time evolution of ESR spectra of DMPO adducts at the cathode side, CCV operation in the in situ FC, with H_2 at the anode. In the top spectrum "0 min" indicates that the spin trap was added just before FC operation, as in Figure 2. Note the dominant DMPO/H adduct when the spin trap was added after 120 min of FC operation together with weak signals from the DMPO/OH adduct (circles); and the appearance of the carbon-centered radical (CCR) adduct (downward arrow points to the low field signal) when the spin trap was added after 240 min of operation. (B) Experimental and simulated ESR spectra of adducts when the spin trap was added after 360 min of operation. The relative intensity of each adduct is shown on the left. Modulation amplitude 0.5 G, receiver gain 1×10^5, 50 scans. See text.

Cathode Side (D_2/O_2). The evolution of ESR spectra when the spin trap was added just before CCV operation and after the indicated operating times is shown in Figure 4A. Immediately after the start of the FC operation, the ESR spectrum consists of two sets of lines: spectrum **1**, the DMPO/OOH (or DMPO/OOD) adduct consists of three doublets with $a_N = 14.0$ G and $a_H = 12.4$ G and is clearly distinguished by the splitting of the two middle signals; spectrum **2**, consisting of three lines, is assigned to the weak signal from DMPO degradation, the triplet due to the radical formed by cleavage of the N−C bond and ring opening, with $a_N \approx 15$ G.[47] In some experiments the DMPO/OH adduct was detected first when the spin trap was added just before the start of the FC operation; for this reason we listed both this adduct and the DMPO/OOH adduct in Table 2. However, in most experiments the DMPO/OOH adduct was detected first; for this reason we presented this situation in Figure 4A.

The signal from DMPO degradation was not mentioned for experiments with H_2 at the anode because the corresponding signals overlap the strong signals from the DMPO/H adduct. This is not the case for the D_2 experiments, Figure 4, where there is no overlap initially (120 min operation).

After 120 min the signal from DMPO degradation is stronger than that of the DMPO/OOH adduct. Additional signals, from adduct **3,** appeared and were assigned to the DMPO/CCR adduct,[27] whose relative intensity is higher after 240 min of FC operation. After 360 min, two additional signals appeared and were assigned to **4,** the DMPO/H adduct, and **5**, the DMPO/D adduct; we marked only the extreme signals for each additional adduct.

The ESR spectrum recorded when the spin trap was added after 360 min of CCV FC operation and the corresponding simulated spectrum are presented in Figure 4B, together with the deconvolution of the simulated spectrum into four components. The dominating contribution (50%) is from the DMPO/OOH adduct with $a_N = 14.1$ G, $a_H = 13.6$ G. The other components are the DMPO/H adduct (25%) with $a_N = 15.9$ G, $a_H = 21.0$ G (2H); the DMPO/D adduct (15%) with $a_N = 15.9$ G, $a_H = 21.0$ G (1H), $a_D = 3.3$ G (1D); and the DMPO/CCR adduct (10%) with $a_N = 15.6$ G, $a_H = 22.0$ G. DMPO/OOH has broader lines compared to those of component **1** in Figure 4A (top spectrum), possibly due to spin−spin interactions. Despite the superposition of four spectral components, the agreement between experimental and simulated spectra in Figure 4B is very good.

With D_2 at the anode, only the DMPO/OOH adduct was detected at the cathode for OCV operation times up to 360 min.

Anode Side (H_2/O_2). Results for CCV and OCV operation of the in situ FC are presented in Figure 5A. Strong signals from the characteristic triplet of triplets of the DMPO/H adduct, with $a_N = 15.8$ G, $a_H = 21.2$ G (2H), were detected for CCV operation. The same signal but with lower intensity was detected after 120 min of CCV operation. As seen in Table 2, a similar adduct but with slightly different ESR parameters ($a_N = 15.2$ G, $a_H = 20.2$ G (2H)) was detected at the cathode side; different local polarities may account for the slightly different magnetic parameters. Weak signals from the DMPO/CCR adduct were also detected at the anode after FC operation times ≥240 min (spectra not given). It is possible that this adduct appears weak because it is obscured by the strong signal from the DMPO/H adduct.

The DMPO/OOH and DMPO/H adducts were detected at the anode for OCV operation.

Anode Side (D_2/O_2). An intense ESR signal was obtained for CCV operation when the DMPO spin trap was deposited at the anode side just before FC operation, as shown in Figure 5B. The spectrum was simulated by a superposition of two components: The dominating component was assigned to the

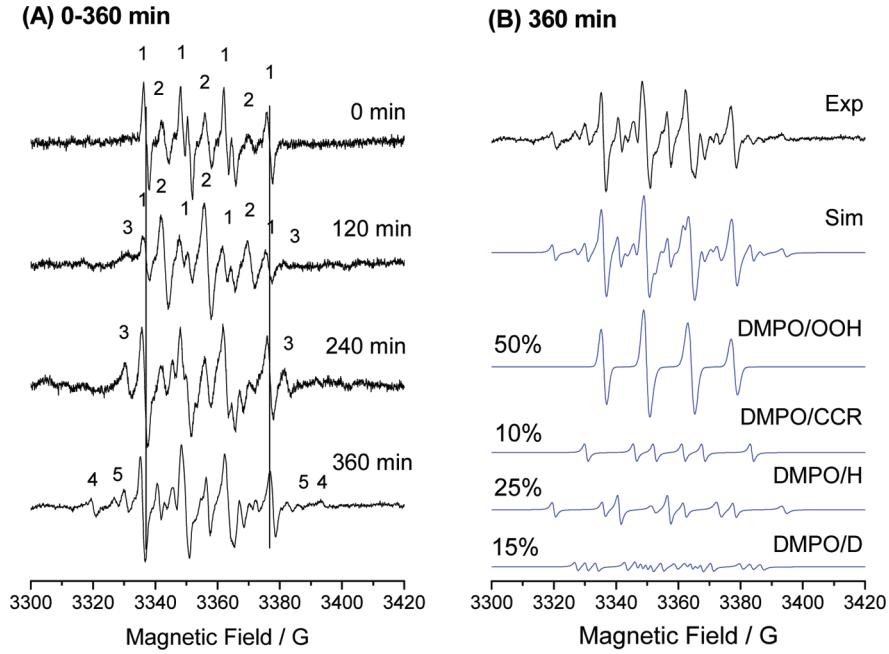

Figure 4. (A) Time evolution of ESR spectra of DMPO adducts at the cathode side in the in situ FC, with D_2 at the anode. In the top spectrum "0 min" indicates that the spin trap was added just before FC operation. The carbon-centered radical (CCR) adduct (3) appeared when the spin trap was added after 120 min of operation. Assignments: 1, DMPO/OOH; 2, DMPO/Degr; 3, DMPO/CCR; 4, DMPO/H; 5, DMPO/D. (B) Experimental and simulated ESR spectra of adducts when the spin trap was added after 360 min of operation. Modulation amplitude 2 G, receiver gain 4.48 × 10^5, 20 scans. See text.

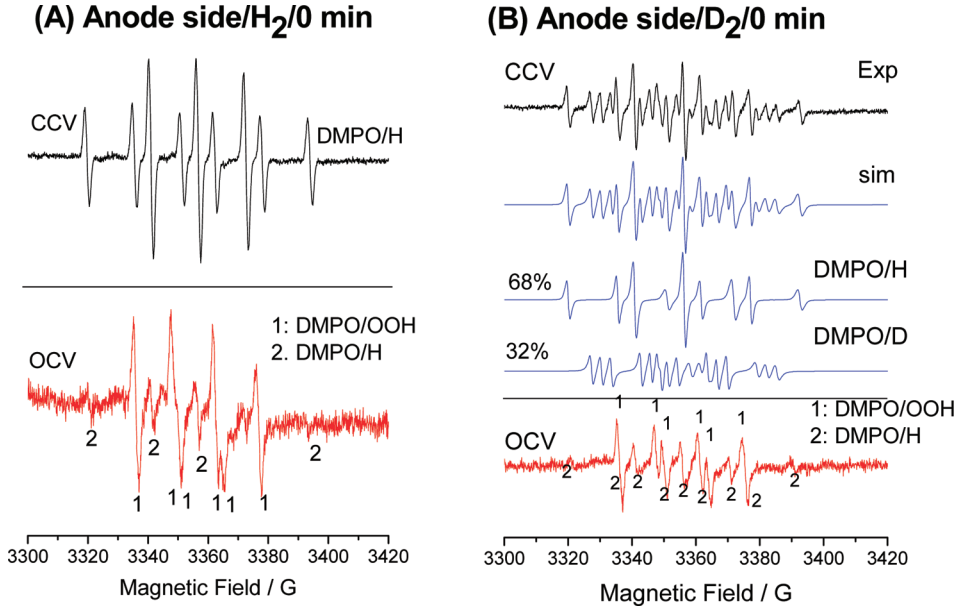

Figure 5. Anode side, comparison of H_2 and D_2. (A) Appearance of the DMPO/H adduct on CCV and OCV conditions, and of the DMPO/OOH adduct only on OCV conditions. The spin trap was added just before FC operation. Only selected lines were numbered for the DMPO/H adduct. (B) Experimental and simulated ESR spectra of DMPO adducts at the anode side, with D_2 at the anode. Note the appearance of both DMPO/H and DMPO/D adducts on CCV FC operation, and of DMPO/OOH and DMPO/H adducts on OCV FC operation. The same adducts were detected when the spin trap was added just before FC operation or after 120 min of operation. Modulation amplitude 1 G, receiver gain 1 × 10^6, 50 scans. See text.

DMPO/H adduct with $a_N = 15.5$ G, $a_H = 21.8$ G (2H) (68%). The additional signal was assigned to the DMPO/D adduct with $a_N = 15.5$ G, $a_H = 21.8$ G, $a_D = 3.2$ G (32%). The same adducts were also detected when DMPO was added after 120 min of fuel cell operation, but with slightly different intensity ratios, 65 and 35%, respectively. The presence of the DMPO/H adduct in experiments with D_2 at the anode will be discussed below.

The DMPO/OOH and DMPO/H adducts were detected for OCV operation of the FC.

In summary: the presence of the DMPO/OOH adduct at the cathode was detected both for CCV and OCV FC conditions. At the anode, however, this adduct was detected only for OCV conditions, thus indicating that the $HOO^{\bullet}$ radicals are generated chemically.

Discussion

The origin of species that contribute to the degradation of the membrane during FC operation has been the focus of

numerous recent studies.[15−20] A basic hypothesis that is generally accepted in the degradation community involves the central role of hydroxyl radicals in the membrane degradation process, an idea that is consistent with the recent thermochemical and kinetic analysis.[11] The results presented above indicate that $HO^{\bullet}$ radicals are formed in the presence of the catalyst at both the anode and cathode via crossover gases, and also by decomposition of H_2O_2, in accord with recent ideas on membrane fragmentation. H_2O_2 is documented to form both chemically at both electrodes via crossover gases, and electrochemically as described in reactions 1−3.[38]

The conclusions that will be derived from this study are based on the detection of the DMPO adducts in the spin-trapping experiments for CCV and OCV FC operating conditions, and their significance in terms of what they tell us about the processes that occur in a FC. The *identification* of adducts will be justified, taking into consideration literature data and our previous spin trapping studies. The role of oxygen radicals and of hydrogen or deuterium atoms in the formation of membrane-derived fragments will also be discussed. At this stage of our work, the focus was on identification of the radicals trapped by DMPO. The relation between the concentration of the radicals scavenged and that of the corresponding adducts when a radical mixture is present may be elusive at this time or at best qualitative, and will drive further experimentation to more accurately describe the system. Several remaining questions are mentioned in the section entitled Unresolved Issues.

The DMPO/OH Adduct. DMPO is known as the spin trap of choice for $HO^{\bullet}$ radicals, with hfs that do not vary significantly in the various systems:[23,25−27,29,36] $a_N \approx a_H \approx 14.8 \pm 0.1$ G. There is no doubt in the identification of this adduct for CCV operation *at the cathode* in the present study, as seen in the spectra shown in Figures 2 and 3A, and in the parameters summarized in Table 2. In Figure 3A, weak signals from the DMPO/OH adduct are still detected in addition to the DMPO/H adduct after 120 min of FC operation and are indicated by circles. The trapping rates of DMPO for scavenging hydrogen atoms and hydroxyl radicals are similar,[48] $\approx 3 \times 10^9$ M^{-1} s^{-1}. Therefore, the relative intensities of these two adducts in Figure 3A are expected to closely represent the corresponding relative *radical intensities*: weak for the hydroxyl radicals and dominant for $H^{\bullet}$. The relative intensities of adducts can also be governed by their stabilities under the conditions prevailing in a fuel cell. The appearance of the DMPO/OH adduct *at the cathode only* is an indicator that its electrochemical formation is a major source for $HO^{\bullet}$ formation for CCV operating conditions.

The DMPO/OOH Adduct. Identification of this adduct in Figure 2 (cathode, OCV), Figure 3 (cathode, CCV), Figure 4 (cathode, CCV), and Figure 5 (anode, OCV) follows most magnetic parameters given in the literature. Slight variations of the ^{14}N and ^{1}H hfs have been detected in numerous studies and have been often assigned to variations in the local polarity. The a_N values in the range 13.7−14.1 G and the a_H values in the range 11.8−13.6 G given in Table 2 are well within published limits.[23,41−45]

In our previous study with DMPO as the spin trap, adducts of both $HOO^{\bullet}$ and $O_2^{\bullet-}$ radicals have been identified, with slightly different a_N and a_H values.[23] In much of the spin-trapping literature these two adducts were assigned the same parameters,[49] because in aqueous systems the hfs are about the same: $a_N \approx 14$ G and $a_H \approx 12$ G. The concentrations of the $HOO^{\bullet}$ and $O_2^{\bullet-}$ radicals are expected to depend on the pH, as seen in reaction 4.

According to a model described in the literature, trapping of $HOO^{\bullet}$ by DMPO predominates below pH = 7.7, and of $O_2^{\bullet-}$ above this pH value.[50] As discussed above, we do not expect the formation of the superoxide radical $O_2^{\bullet-}$ at the low pH of a fuel cell. Therefore, the identification of the DMPO/OOH adduct stands, both from consideration of the spin-trapping literature and from expected conditions in a fuel cell. We notice also the very high resolution in the spectrum of this adduct, especially when the radical concentration is low. The best resolution is seen when the FC is run with both H_2 and D_2, for example in the spectra shown in Figure 2 (OCV, H_2 at the anode), and in Figure 4A (CCV, D_2 at the anode), suggesting that we cannot distinguish whether the trapped radical is $DOO^{\bullet}$, or $HOO^{\bullet}$ based on line widths.

The identification of the $HOO^{\bullet}$ adduct at the anode formed via reactions 8 due to crossover of O_2 is in line with current results.[51,52] We note that the presence of $HOO^{\bullet}$ and $O_2^{\bullet-}$ DMPO adducts was mentioned in ex situ experiments of a Nafion dispersion exposed to the Fenton reagent, but in the authors' words, "Due to overlap of the spectra it is not possible to observe all lines or to measure the splitting constants precisely...".[53]

As we have detected the presence of $H^{\bullet}$ and $D^{\bullet}$ adducts at both cathode and anode sides, we will discuss the formation of $HOO^{\bullet}$ via these atoms in the following section.

The DMPO/H and DMPO/D Adducts. The identification of these adducts is based on the spin-trapping database[30] and refs 38−40. With H_2 gas fed at the anode, the DMPO/H adduct was detected *at the anode*, as seen in Figure 5A; a weak signal from the CCR adduct was detected after prolonged FC operation, ≥240 min. With D_2 gas fed at the anode, both the DMPO/D and the DMPO/H adducts were detected *at the anode* for similar operating condition, and also when the spin trap was added after 120 min of CCV FC operation (Figure 5B). The detection of the DMPO/CCR adduct is considered impossible in the spectra presented in Figure 5B, because of the strong signals from the DMPO/H and DMPO/D adducts. A less intense signal from the DMPO/H adduct was also detected at the anode for OCV FC operation, alongside the DMPO/OOH adduct, with either H_2 or D_2 fed at the anode.

The appearance of the DMPO/H adduct at the anode, Figure 5A, and of the DMPO/D adduct, Figure 5B, in the presence of H_2 or D_2 gases, respectively, fed at the anode can be explained by the reactions 4 and 5 above: chemical formation of $HO^{\bullet}$ (reaction 4), which then reacts with H_2 to generate the DMPO/H adduct.

The DMPO/H and DMPO/D adducts were also detected at the cathode when the spin trap was added after 120−360 min of CCV operation, Figures 3 and 4, respectively: Figure 3B presents results at the cathode after 360 min of FC operation with H_2 at the anode; the relative intensity of the DMPO/H adduct is 36%. Figure 4 shows the appearance of *both* DMPO/H and DMPO/D adducts at the cathode after 360 min of CCV FC operation with D_2 at the anode.

In experiments with α-(4-pyridyl-1-oxide)-*N*-*tert*-butylnitrone (POBN) as the spin trap, Panchenko et al. did not detect the formation of the POBN/D adduct in an in situ FC with deuterium at the anode; the POBN/D adduct was detected, however, when H_2O was replaced by D_2O and hydrogen was fed at the anode.[36] The authors explained their result by assuming that the POBN spin trap was first reduced to its anion at the electrode surface, followed by protonation by solvent molecules (H_2O or D_2O). This approach may be valid for POBN as the spin probe. For DMPO, however, the work of Endo et al. provides the conclusive proof that DMPO is not reduced to the corresponding

anion in an electrochemical reaction that took place in a specially designed ESR cell;[40,41] therefore we can conclude that the DMPO/H adduct is not formed by the reduction of DMPO, but by spin trapping of the hydrogen atom. Taken together, the appearance of the DMPO/H (for H_2 at the anode) and DMPO/D (for D_2 at the anode) indicate the formation of H$^\bullet$ or D$^\bullet$, respectively, followed by spin trapping.

The appearance of the DMPO/H adduct for D_2 at the anode, Figures 4B and 5B, cannot be explained by reaction 5 above, and encourages us to invoke an additional process, which may involve reduction of H_3O^+: $H_3O^+ + e^- \rightarrow H_2O + H^\bullet$. We note that the typical current density in our experiments is 4−15 μA/cm^2; the area and mass of the membrane are ≈0.5 cm^2 and 35 mg, respectively. Under these conditions, the expected amount of D_2O formed when D_2 is fed at the anode is only <1 mg after several hours of FC operation. The total expected amount of water (15−20%) is 5−7 mg water. This rationale may explain the formation of both DMPO/H and DMPO/D adducts, as detected in Figure 4A,B. Atom recombination and crossover should also be considered and may explain the results shown in Figure 5B. However, the potential for H_3O^+ reduction is high, >2 V. For this reason, the appearance of the DMPO/H adduct for D_2 at the anode appears to be still an unresolved issue that needs additional experimentation.

The relative reactivity of the spin trap toward hydrogen and deuterium atoms is an issue that we plan to study in the future. Some observations in the present study suggest that the spin trap reactivity is an important factor that determines the relative intensity of adducts. In repeat experiments we have observed some variations of the relative intensities of adducts; this result may be due to variations in the local concentration of the spin trap on the MEA, because the least quantitative step in the in situ FC operation is the addition of the spin trap solution. For example, for results presented in Figure 4A, we have detected either DMPO/OH or DMPO/OOH adducts, see Table 2; variations in the adduct intensity with spin trap concentration are expected when the rates of scavenging of radicals in a mixture are different.

The effect of H$^\bullet$ or D$^\bullet$ presence *at both anode and cathode* will be discussed below, in connection with the detection of the DMPO/CCR adduct.

Detection of a Membrane-Derived Spin Adduct. The identification of the DMPO/CCR adduct at the cathode after 240 min of CCV FC operation with H_2 at the anode, Figure 3, and after 120 min of CCV operation with D_2 at the anode is based on our work and numerous studies.[23,27,30] DMPO is an important spin trap for the detection of CCRs, because the hfs from Hβ is larger than that measured for adducts of oxygen-centered radicals (OCR), typically ≥20 G in DMPO/CCR compared to ≈12−15 G for DMPO/OCR. The parameters for DMPO/CCR in the in situ FC are close to one of the two DMPO/CCR adducts detected in perfluoro(2-ethoxyethane)-sulfonic acid, $CF_3CF_2OCF_2CF_2SO_3H$ (PFEESA), when exposed to HO$^\bullet$ radicals generated by UV irradiation of H_2O_2.[27] As PFEESA was selected as a model compound for the behavior of the Nafion side chain, it is possible that the CCR adduct detected in this study is also derived from the side chain. We note that this adduct was detected at 300 K, suggesting that membrane fragmentation can be detected by ESR at temperatures well below the typical operating temperature of FCs, ≈350 K.

Membrane fragmentation by attack of HO$^\bullet$ radicals can lead to chain unzipping, a mechanism that is widely published in the literature.[17−19] In addition, our work with model compounds has implicated HO$^\bullet$ radicals in reactions with the sulfonic groups.[27] The hydrogen or deuterium radicals, H$^\bullet$ or D$^\bullet$, detected in the in situ FC are reactive species with a standard reduction potential of 2.3 V vs the standard hydrogen electrode (SHE) and can potentially abstract fluorine atoms from the tertiary C−F bond of the membrane, leading to chain scission. The reactivity of H$^\bullet$ toward abstraction of fluorine atoms is thermodynamically driven by the formation of the very strong H−F bond (571 kJ/mol).[11] Hydroxyl radicals cannot abstract fluorine atoms from fluorocarbons because the HO−F bond is rather weak, making the reaction very endothermic (270 kJ/mol). On the other hand, abstraction of fluorine by the hydrogen atom is exothermic (−85 kJ/mol) and kinetically feasible. This process is expected at both the anode and cathode, and is supported by our results: the DMPO/CCR adduct was clearly detected at the cathode (Figures 3 and 4), and weak signals were also detected at the anode after FC operation of ≥240 min. We plan to study conditions that may affect the appearance of this adduct at the anode after long time FC operation.

TABLE 3: Processes Suggested by the in Situ Fuel Cell Experiments

results	processes	
	$O_2 + 2H^+ + 2e^- \rightarrow H_2O_2$ (electrochemical H_2O_2 formation)	(1)
HO$^\bullet$/CCV/cathode Figure 2	$H_2O_2 \rightarrow 2\ HO^\bullet$ (electrochemical HO$^\bullet$ formation)	(2)
HOO$^\bullet$/CCV/cathode Figure 3	$H_2O_2 + HO^\bullet \rightarrow HOO^\bullet + H_2O$ (electrochemical HOO$^\bullet$ formation)	(3)
leading to H$^\bullet$ or D$^\bullet$ OCV/anode Figure 5	$H_2 + O_2 \rightarrow 2HO^\bullet$ (chemical HO$^\bullet$ formation on catalyst)	(4)
H$^\bullet$/CCV/cathode/anode Figures 3, 4	$HO^\bullet + H_2\ (D_2) \rightarrow H_2O + H^\bullet\ (D^\bullet)$ (chemical H$^\bullet$ and D$^\bullet$ formation)	(5)
HOO$^\bullet$/OCV/cathode Figure 3	$H^\bullet + O_2 \rightarrow HOO^\bullet$ (chemical HOO$^\bullet$ formation)	(6)

Separate Detection of Radicals and Membrane-Derived Fragments at the Anode and Cathode. Analysis of the DMPO adducts leads to the conclusion that it is possible to examine separately processes that occur at the electrodes: for example, the data presented above have shown that the DMPO/OH and DMPO/CCR adducts appear *only at cathode*, during CCV operation. This observation also means that the spin trap and the corresponding adducts do not diffuse from one electrode to another.

At the anode, the DMPO/OOH, DMPO/H, and DMPO/D adducts were detected. Analysis of the results for these adducts made possible the detection of crossover processes: of O_2 from the cathode to the anode, thus explaining the formation of the DMPO/OOH adduct (reaction 6); and of H_2 and D_2 from the anode to the cathode, thus explaining the presence of DMPO/H at the anode and the cathode.

The crossover reactions, reactions at the catalyst, and the formation of H$^\bullet$ or D$^\bullet$ radicals detected as adducts in the present in situ experiments cannot occur in laboratory experiments. Therefore, an important conclusion is that the results presented here suggest different degradation paths for in situ conditions, compared to ex situ studies.

Table 3 summarizes the processes suggested by the results presented in Figures 2−5 and in Table 2.

Unresolved Issues and Follow-up Studies. While this study has provided a picture on the formation of radicals and crossover

processes in the in situ FC, it has also raised some questions that we plan to consider in our next experiments:

(a) An important focus in our future experiments will be an assessment of the relative reactivity of the spin trap toward different radicals in a mixture.[33,34] These experiments are expected to be easier to perform in liquid solutions with model compounds, of the type published in our recent study.[27] The results may lead to a better evaluation of the relative concentrations of radicals, not adducts, formed.

(b) The carbon-centered radical adduct, DMPO/CCR, was detected at the cathode side. The similarity of the ^{14}N and Hβ hfs with PFEESA as the model compound suggests that it may be derived from the side chain. Use of 2-methyl-2-nitrosopropane (MNP) as the spin trap may provide the answer because this spin has the potential to detect hfs from ^{19}F nuclei,[27] and such experiments are included in our future plans.

(c) The CCR adduct at the anode is weak. Its very presence can be considered as an indicator of the contribution of H$^\bullet$ to membrane fragmentation. We plan to complement this study by looking at the factors that may affect the intensity of the DMPO/CCR adduct at the anode.

(d) In Table 2, some of the g values are about 2.0040, lower than those expected for nitroxide radicals. The significance of this result will be searched, both data in the spin-trapping database[33] and in additional spin-trapping studies in our laboratory.

(e) So far we have not been able to provide a fully satisfying explanation for the appearance of the DMPO/H adduct when the FC was operated with deuterium at the anode. This topic will be explored further, for example, in single-sided MEA studies, by identifying the parameters that influence the appearance of this adduct. Such studies are expected to distinguish between crossover processes and chemical reactions.

Summary and Conclusions

We have presented experiments in an in situ fuel cell inserted in the resonator of an ESR spectrometer that offered the ability to monitor processes leading to the formation of oxygen radicals, hydrogen and deuterium atoms, and radical fragments derived from the membrane. The in situ fuel cell was operated at 300 K with a Nafion 117 membrane covered on both sides by Pt as catalyst (coverage 0.2 mg/cm^2), at closed circuit voltage (CCV) and open circuit voltage (OCV) conditions. Experiments with hydrogen or deuterium at the anode, and oxygen at the cathode, were performed. The presence of the radicals was determined by addition of 5,5-dimethylpyrroline *N*-oxide (DMPO) as a spin trap, simulation of the spectra from the DMPO adducts, and analysis of the corresponding magnetic parameters.

The DMPO/OH adduct was detected *only at the cathode, for CCV operation,* suggesting electrochemical formation of HO$^\bullet$ by the two-electron reduction of oxygen. DMPO adducts of H$^\bullet$ and D$^\bullet$ atoms were detected at the cathode for CCV operation, and at the anode after both CCV and OCV operations. Only the DMPO/H adduct was detected when the fuel cell was operated with hydrogen at the anode; with deuterium at the anode, however, both DMPO/H and DMPO/D adducts were detected at the anode. The DMPO/OOH adduct was identified in this study for the first time in a fuel cell, and appeared at the cathode for CCV and OCV operation, and anode for OCV operation.

Adducts of carbon-centered radicals (CCRs) were detected *at the cathode* after 240−360 min of CCV FC operation at 300 K; weaker signals from these adducts were also detected at the anode. The CCRs can be derived only from the membranes, and their detection indicates that membrane fragmentation can occur even below the typical operating temperature of FCs, ≈350 K. The magnetic parameters of the CCR adduct were compared with those detected for DMPO/CCR adducts in perfluoro(2-ethoxyethane)sulfonic acid, $CF_3CF_2OCF_2CF_2SO_3H$ (PFEESA), a model compound for the side chain of Nafion, when exposed to HO$^\bullet$ radicals. The similarity of the hfs may indicate that CCR radicals in the in situ fuel cell are also derived from the side chain.

The in situ results point to crossover processes, reactions at the catalyst surface, and the involvement of H$^\bullet$ and D$^\bullet$ atoms in attack on the membrane, which are not possible in ex situ studies. Therefore, different membrane degradation mechanisms in the two types of experiments can be expected.

Acknowledgment. This study was supported by the General Motors Fuel Cell Research Lab and by the Polymers Program of the National Science Foundation. We are grateful to Dr. Cortney Mittelsteadt of Giner Electrochemical Systems LLC for the gift of the MEAs based on Nafion 117 membranes.

References and Notes

(1) Fuel Cells—Green Power, Los Alamos National Laboratory. See also website:www.education.lanl.gov/resources/fuelcells.

(2) CUTE website: www.fuel-cell-bus-club.com.

(3) *Ionomers: Characterization, Theory, and Applications*; Schlick, S., Ed.; CRC Press: Boca Raton, FL, 1996; 300 pp.

(4) Risen, W. M., Jr. In *Ionomers: Characterization, Theory, and Applications*; Schlick, S., Ed.; CRC Press: Boca Raton, FL, 1996; Chapter 12, pp 281−300.

(5) Cappadonia, M.; Erning, J. W.; Niaki, M. S.; Stimming, U. *Solid State Ionics* **1995**, *77*, 65–69.

(6) Paddison, S. J. *Ann. Rev. Mater. Res.* **2003**, *33*, 289–319.

(7) Huang, C.; Tan, K. S.; Lin, J.; Tan, K. L. *Chem. Phys. Lett.* **2003**, *371*, 80–85.

(8) Adzic, R. In *Electrocatalysis*; Lipkowski, J., Ross, P. N., Eds.; Wiley-VCH: New York, 1998; pp 197−242.

(9) Pozio, A.; Silva, R. F.; De Francesco, M.; Giorgi, L. *Electrochim. Acta* **2003**, *48*, 1543–1549.

(10) Sethuraman, V. A.; Weidner, J. W.; Haug, A. T.; Motupally, S.; Protsailo, L. V. *J. Electrochem. Soc.* **2008**, *155*, B50−B57.

(11) Coms, F. D. *ECS Trans.* **2008**, *16* (2), 235–255.

(12) (a) Walling, C. *Acc. Chem. Res.* **1975**, *8*, 125–131. (b) Sawyer, D. T.; Sobkowiak, A.; Matsushita, T. *Acc. Chem. Res.,* **1996**, *29*, 409–416. (c) Walling, C. *Acc. Chem. Res.* **1998**, *31*, 155–157. (d) Goldstein, S.; Meyerstein, D. *Acc. Chem. Res.* **1999**, *32*, 547–550.

(13) (a) Miyatake, K.; Oyaizu, K.; Tsuchida, E.; Hay, A. S. *Macromolecules* **2001**, *34*, 2065–2071. (b) Fang, J.; Guo, X.; Harada, S.; Watari, T.; Tanaka, K.; Kita, H.; Okamoto, K. *Macromolecules* **2002**, *35*, 9022–9028.

(14) Bednarek, J.; Schlick, S. *J. Phys. Chem.* **1991**, *95*, 9940–9944.

(15) Borup, R.; Meyers, J.; Pivovar, B.; Kim, Y. S.; Mukundan, R.; Garland, N.; Myers, D.; Wilson, M.; Garzon, F.; Wood, D.; Zelenay, P.; More, K.; Stroh, K.; Zawodinski, T.; Boncella, J.; McGrath, J. E.; Inaba, M.; Miyatake, K.; Hori, M.; Ota, K.; Ogumi, Z.; Miyata, S.; Nishikate, A.; Siroma, Z.; Uchimoto, Y.; Yasuda, K.; Kimijima, K. I.; Iwashita, N. *Chem. Rev.* **2007**, *107*, 3904–3951.

(16) Liu, W.; Ruth, K.; Rusch, G. *J. New Mater. Electrochem. Syst.* **2001**, *4*, 227–232.

(17) Curtin, D. E.; Lousenberg, R. D.; Henry, T. J.; Tangeman, P. C.; Tisack, M. E. *J. Power Sources* **2004**, *131*, 41–48.

(18) Healy, J.; Hayden, C.; Xie, T.; Olson, K.; Waldo, R.; Brundage, A.; Gasteiger, H.; Abbott, J. *Fuel Cells* **2005**, *5*, 302–308.

(19) Xie, T.; Hayden, C. *Polymer* **2007**, *48*, 5497–5506.

(20) Zhou, C.; Guerra, M. A.; Qiu, Z.-M.; Zawodzinski, T. A.; Schiraldi, D. A. *Macromolecules* **2007**, *40*, 8695–8707.

(21) Bosnjakovic, A.; Schlick, S. *J. Phys. Chem. B* **2004**, *108*, 4332–4337.

(22) Kadirov, M. K.; Bosnjakovic, A.; Schlick, S. *J. Phys. Chem. B* **2005**, *109*, 7664–7670.

(23) Bosnjakovic, A.; Schlick, S. *J. Phys. Chem. B* **2006**, *110*, 10720–10728.

(24) Lund, A.; Macomber, L.; Danilczuk, M.; Stevens, J.; Schlick, S. *J. Phys. Chem. B* **2007**, *111*, 9484–9491.

(25) Danilczuk, M.; Bosnjakovic, A.; Kadirov, M. K.; Schlick, S. *J. Power Sources* **2007**, *172*, 78–82.

(26) Roduner, E.; Schlick, S. In *Advanced ESR Methods in Polymer Research*; Schlick, S., Ed.; Wiley: Hoboken, NJ, 2006; *Chapter 8*, pp 197−228.

(27) Danilczuk, M.; Coms, F. D.; Schlick, S. *Fuel Cells* **2008**, *8* (6), 436–452.

(28) Janzen, E. G. *Acc. Chem. Res.* **1971**, *4*, 31–40.

(29) Lagercrantz, C. *J. Phys. Chem.* **1971**, *75*, 3466–3475.

(30) Spin Trapping Database, http://EPR.niehs.nih.gov.

(31) Ghassemzadeh, L.; Marrony, M.; Barrera, R.; Kreuer, K. D.; Maier, J.; Müller, K. *J. Power Sources* **2009**, *186*, 334–338.

(32) Haire, D. L.; Hilborn, J. W.; Janzen, E. G. *J. Org. Chem.* **1986**, *51*, 4298–4300.

(33) The software WinSim can be accessed at: http://www.niehs.nih.gov/research/resources/software/tools/index.cfm.

(34) Villamena, F. A.; Haddad, C. M.; Zweier, J. L. *J. Chem. Phys. A* **2003**, *107*, 4407–4414.

(35) Villamena, F. A.; Haddad, C. M.; Zweier, J. L. *J. Phys. Chem. A* **2005**, *109*, 1662–1674.

(36) Panchenko, A.; Dilger, H.; Kerres, J.; Hein, M.; Ullrich, A.; Kaz, T.; Roduner, E. *Phys. Chem. Chem. Phys. (PCCP)* **2004**, *6*, 2891–2894.

(37) Panchenko, A.; Dilger, H.; Moller, E.; Sixt, T.; Roduner, E. *J. Power Sources* **2004**, *127*, 325–330.

(38) Mittal, V. O.; Kunz, H. R.; Fenton, J. M. *J. Electrochem. Soc.* **2007**, *154* (7), B652–B656.

(39) Makino, K.; Mossoba, M. M.; Riesz, P. *J. Phys. Chem.* **1983**, *87*, 1369–1377.

(40) Endo, N.; Higashi, K.; Tajima, K.; Makino, K. *Chem. Lett.* **2001**, 548–549.

(41) Endo, N.; Higashi, K.; Kanaori, K.; Tajima, K.; Makino, K. *Bull. Chem. Soc. Jpn.* **2002**, *75*, 149–150.

(42) Kalyanaraman, B.; Mottley, C.; Mason, R. P. *J. Biochem. Biophys. Methods* **1984**, *9*, 27–31.

(43) Dikalov, S. I.; Mason, R. P. *Free Radical Biol. Med.* **1999**, *27*, 864–872.

(44) Dikalov, S. I.; Mason, R. P. *Free Radical Biol. Med.* **2001**, *30*, 187–197.

(45) Thomas, C. E.; Morehouse, L. A.; Aust, S. D. *J. Biol. Chem.* **1985**, *260*, 3275–3280.

(46) Reszka, K.; Lown, J. W.; Chignell, C. F. *Photochem. Photobiol.* **1992**, *55*, 359–366.

(47) Hawkins, C. L.; Davies, M. J. *Biochem. J.* **1999**, *340*, 539–548.

(48) Madden, K. P.; Taniguchi, H. *J. Phys. Chem.* **1996**, *100*, 7511–7516.

(49) Rosen, G. M.; Britigan, B. E.; Halpern, H. J.; Pou, S. *Free Radicals: Biology and Detection by Spin Trapping*; Oxford University Press: New York, 1999.

(50) Finkelstein, E.; Rosen, G. M.; Rauckman, E. J. *Arch. Biochem. Biophys.* **1980**, *200*, 1–16.

(51) LaConti, A. B.; Hamdan, M.; McDonald, R. C. In *Handbook of Fuel Cells−Fundamentals, Technology and Applications*; Vielstich, W., Gasteiger, H. A., Lamm, A., Eds.; John Wiley & Sons: New York, 2003; Vol. 3, pp 647−662.

(52) Anderson, A. B.; Albu, T. V. *J. Electrochem. Soc.* **2000**, *147*, 4229–4238.

(53) Vogel, B.; Aleksandrova, E.; Mitov, S.; Krafft, M.; Dreizler, A.; Kerres, J.; Hein, M.; Roduner, E. *ECS Trans.* **2007**, *11* (1), 1105–1114.

JP901597F